arXiv:1303.7096v1 [math.GT] 28 Mar 2013

COMPLEX HYPERBOLIC GEOMETRY OF THE FIGURE EIGHT KNOT

MARTIN DERAUX AND ELISHA FALBEL

Abstract. We show that the figure eight knot complement admits a unique complete spherical CR structure with unipotent boundary holonomy.

1. Introduction

The general framework of this paper is the study of the interplay between topological properties of 3-manifolds and the existence of geometric structures. The model result along these lines is of course Thurston's geometrization conjecture, recently proved by Perelman, that contains a topological characterization of manifolds that admit a geometry modeled on real hyperbolic space $\mathbf{H}^3_{\mathbb{R}}$. Beyond an existence result (under the appropriate topological assumptions), the hyperbolic structures can in fact be constructed fairly explicitly, as one can easily gather by reading Thurston's notes [16], where a couple of explicit examples are worked out.

The idea is to triangulate the manifold, and to try and realize each tetrahedron geometrically in $\mathbf{H}^3_{\mathbb{R}}$. The gluing pattern of the tetrahedra imposes compatibility conditions on the parameters of the tetrahedra, and it turns out that solving these compatibility equations is very often equivalent to finding the hyperbolic structure. Over the years, this procedure has been made completely general and effective (at least for manifolds that can be triangulated with a fairly small number of tetrahedra), and it can now be used routinely by any mathematician by running the SnapPea software.

In this paper, we are interested using the 3-sphere S^3 as the model geometry, with the natural structure coming from describing it as the boundary of the unit ball $\mathcal{B}^2 \subset \mathbb{C}^2$. Any real hypersurface in $\mathbb{C}^2$ inherits what is called a CR structure (the largest subbundle in the tangent bundle that is invariant under the complex structure), and such a structure is called spherical when it is locally equivalent to the CR structure

Date: Mar 27, 2013.

of S^3. Local equivalence with S^3 in the sense of CR structures translates into the existence of an atlas of charts with values in S^3, and with transition maps given by restrictions of biholomorphisms of $\mathcal{B}^2$, i.e. elements of $\mathbf{PU}(2,1)$, see [2].

In other words, a spherical CR structure is a (G,X)-structure with $G = \mathbf{PU}(2,1)$, $X = S^3$. The central motivating question is to give a characterization of 3-manifolds that admit a spherical CR structures - the only known examples known not to carry any spherical CR structure are T^2-bundles over S^1 with hyperbolic gluing map [6].

An important class of spherical CR structures is obtained from discrete subgroups $\Gamma \subset \mathbf{PU}(2,1)$ by taking the quotient of the domain of discontinuity Ω by the action of Γ. These are called complete spherical CR structures, they are the ones that are uniformized by an open set in S^3.

Of course one also wonders which manifolds admit complete spherical CR structures, and to what extent it really makes a difference to require completeness. For instance, when Γ is a finite group acting without fixed points on S^3, $\Omega = S^3$ and $\Gamma \setminus S^3$ gives the simplest class of examples (including lens spaces).

The class of circle bundles over surfaces has been widely explored, and many such bundles are known to admit complete spherical CR structures, see the introduction of [15] and the references given there. It is also known that well-chosen deformations of triangle groups produce spherical CR structures on more complicated 3-manifolds, including real hyperbolic ones. Indeed, Schwartz showed in [13] that the Whitehead link complement admits a complete spherical CR structure, and in [14] he found an example of a closed hyperbolic manifold that arises as the boundary of a complex hyperbolic surface. Once again, we refer the reader to the [15] for a detailed overview of the history of this problem, and also [10] for recent developments.

All these examples are obtained by analyzing special classes of discrete groups, and checking the topological type of their manifold at infinity. In the opposite direction, given a 3-manifold M, one would like a method to construct (and possibly classify) all structures on M, in the spirit of the constructive version of hyperbolization alluded to early in this introduction.

A step in that direction was proposed by the second author in [4], based on triangulations and adapting the compatibility equations to the spherical CR setting. Here a basic difficulty is that there is no canonical way to associate a tetrahedron to a given quadruple of points in S^3. Even the 1-skeleton is elusive, since arcs of $\mathbb{C}$-circles (or $\mathbb{R}$-circles) between two points are not unique (see section 2.1 for definitions).

A natural way over this difficulty is to formulate compatibility conditions that translate the possibility of geometric realization in S^3 only on the level of the vertices of the tetrahedra. Indeed, ordered generic quadruples of points are parametrized up to isometry by appropriate cross ratios, and one can easily write down the corresponding compatibility conditions explicitly [4].

Given a solution of these compatibility equations, one always gets a representation $\rho : \pi_1(M) \to \mathbf{PU}(2,1)$, but it is not clear whether or not the quadruples of points can be extended to actual tetrahedra in a ρ-equivariant way (in other words, it is not clear whether or not ρ is the holonomy of an actual structure).

There are many solutions to the compatibility equations, so we will impose a restriction on the representation ρ, namely that $\rho(\pi_1(T))$ be unipotent for each torus boundary component T of M. This is an extremely stringent condition, but it is natural since it holds for complete hyperbolic metrics of finite volume.

For the remainder of the paper, we will concentrate on a specific 3-manifold, namely the figure eight knot complement, and give encouraging signs for the philosophy outlined over the preceding paragraphs. Indeed, for that specific example, we will check that the solutions to the compatibility equations give one and only one boundary unipotent complete spherical CR structure on the figure eight knot complement (in fact one gets one structure for each orientation on M, see section 9).

We work with the figure eight knot complement partly because it played an important motivational role in the eighties for the development of real hyperbolic geometry. It is well known that this non-compact manifold M admits a unique complete hyperbolic metric, with one torus end (corresponding to a tubular neighborhood of the figure eight knot).

It is also well known that M can be triangulated with just two tetrahedra (this triangulation is far from simplicial, but this is irrelevant in the present context). The picture in Figure 1 can be found for instance in the first few pages of Thurston's notes [16]. The above decomposition can be realized geometrically in $\mathbf{H}^3_{\mathbb{R}}$ (and that the corresponding geometric tetrahedra are regular tetrahedra, so the volume of this metric is $6\mathcal{J}(\pi/3) \approx 2.029$).

For the specific triangulation of the figure eight knot complement depicted in Figure 1, it turns out there are only three solutions to the compatibility equations (up to complex conjugation of the cross ratio parametrizing the tetrahedra), yielding three representations ρ_1, ρ_2 and $\rho_3 : \pi_1(M) \to \mathbf{PU}(2,1)$ (in fact six representations, if we include their

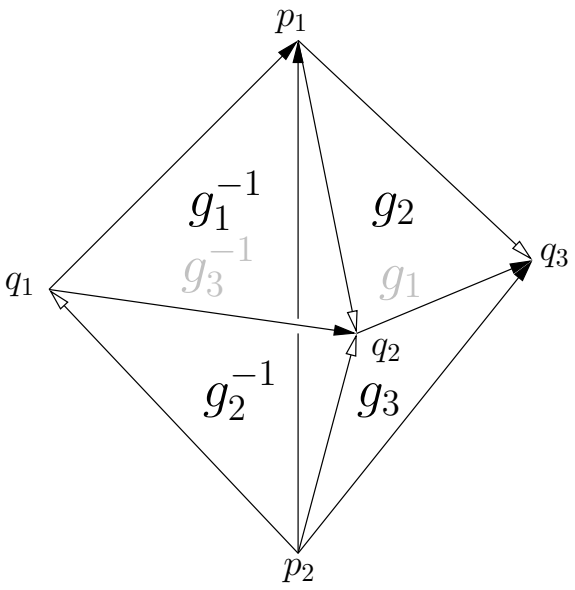

FIGURE 1. The figure eight knot complement can be obtained by gluing two tetrahedra (a face on the left and a face on the right are identified if the corresponding pattern of arrows agree), and removing the vertices.

complex conjugates). Throughout the paper, we will denote by Γ_k the image of ρ_k.

It was shown in [4] that ρ_1 is the holonomy of a *branched* spherical CR structure (the developing map is a local diffeomorphism away from a curve), and that the limit set of Γ_1 is equal to $\partial_\infty \mathbf{H}^2_{\mathbb{C}}$, hence the quotient $\Gamma_1 \setminus \mathbf{H}^2_{\mathbb{C}}$ has empty manifold at infinity. In particular, the corresponding structure is of course not complete. In [5], a branched structure with holonomy ρ_2 is constructed, which is again not complete.

The main goal of this paper is to show that both other representations are holonomy representations of complete unbranched spherical CR structures on the figure eight knot complement. The representations ρ_2 and ρ_3 are not conjugate in $\mathbf{PU}(2,1)$ (their precise relationship will be explained in section 8), but it turns out that the images Γ_2 and Γ_3 are in fact conjugate. Throughout the paper, we will denote by Γ the group Γ_2.

Theorem 1.1. *The domain of discontinuity Ω of Γ is non empty. The action of Γ has no fixed points in Ω, and the quotient $\Gamma \setminus \Omega$ is homeomorphic to the figure eight knot complement.*

One way to formulate this result is that $\Gamma \setminus \mathbf{H}^2_{\mathbb{C}}$ is a complex hyperbolic orbifold whose manifold at infinity is homeomorphic to the figure eight knot complement. The fact that the end of $\Gamma \setminus \mathbf{H}^2_{\mathbb{C}}$ is indeed a manifold, and not just an orbifold, follows from the fact that every elliptic element in Γ has an isolated fixed point in $\mathbf{H}^2_{\mathbb{C}}$ (we will be able to list all conjugacy classes of elliptic elements, by using the cycles of the fundamental domain, see Proposition 5.2).

The relationship between the two structures corresponding to ρ_2 and ρ_3 will be explained by the existence of an orientation-reversing diffeomorphism of the figure eight knot complement (which follows from the fact that this knot is amphichiral). Indeed, given a diffeomorphism $\varphi : M \to \Gamma_2 \setminus \Omega_2$, and an an orientation-reversing diffeomorphism $\tau : M \to M$, $\tau \circ \phi$ defines a spherical CR structure on M with the opposite orientation.

We will see that ρ_2 and ρ_3 are obtained from each other by this orientation switch (see section 8). For that reason, we will work with only one representation for most of the paper, namely ρ_2 (the corresponding statement for ρ_3 will follow by basic orientation considerations).

The result of Theorem 1.1 is stated in terms of the domain of discontinuity which is contained in $\partial_\infty \mathbf{H}^2_{\mathbb{C}}$, so one may expect the arguments to use properties of $S^3 \subset \mathbb{C}^2$ or Heisenberg geometry (see section 2.1). In fact the bulk of the proof is about the relevant complex hyperbolic orbifold $\Gamma \setminus \mathbf{H}^2_{\mathbb{C}}$, and for most of the paper, we will use geometric properties of $\mathbf{H}^2_{\mathbb{C}}$.

The basis of our study of the manifold at infinity will be the Dirichlet domain for Γ_2 centered at a strategic point, namely the isolated fixed point of $G_2 = \rho_2(g_2)$ (we use similar notation for other generators, $\rho_2(g_k) = G_k$). This domain is not a fundamental domain for the action of Γ (the center is stabilized by a cyclic group of order 4), but it is convenient because it has very few faces (in fact all its faces are isometric to each other). In particular, we get an explicit presentation for Γ, given by

$$\langle\, G_1, G_2 \mid G_2^4,\ (G_1G_2)^3,\ (G_2G_1G_2)^3 \,\rangle \tag{1}$$

From this it is easy to determine normal generators for the kernel of ρ_2, see Proposition 5.3.

Acknowledgements: This work was supported in part by the ANR through the project Structure Géométriques et Triangulations. The authors also wish to thank Christine Lescop, Antonin Guilloux, Julien Marché, Jean-Baptiste Meilhan, Pierre Will and Maxime Wolff for useful discussions related to the paper.

2. Basics of complex hyperbolic geometry

2.1. **Complex hyperbolic geometry.** In this section we briefly review basic facts and notation about the complex hyperbolic plane. For much more information, see [7].

We denote by $\mathbb{C}^{2,1}$ the three dimensional complex vector space $\mathbb{C}^3$ equipped with the Hermitian form

$$\langle Z, W\rangle = Z_1\overline{W}_3 + Z_2\overline{W}_2 + Z_3\overline{W}_1.$$

The subgroup of $GL(3,\mathbb{C})$ preserving the Hermitian form $\langle\cdot,\cdot\rangle$ is denoted by $\mathbf{U}(2,1)$, and it acts transitively on each of the following three sets:

$$V_+ = \{Z \in \mathbb{C}^{2,1} : \langle Z, Z\rangle > 0\},$$

$$V_0 = \{Z \in \mathbb{C}^{2,1} - \{0\} : \langle Z, Z\rangle = 0\},$$

$$V_- = \{Z \in \mathbb{C}^{2,1} : \langle Z, Z\rangle < 0\}.$$

Let $P : \mathbb{C}^{2,1} - \{0\} \to \mathbf{P}^2_{\mathbb{C}}$ be the canonical projection onto complex projective space, and let $\mathbf{PU}(2,1)$ denote the quotient of $U(2,1)$ by scalar matrices, which acts effectively on $\mathbf{P}^2_{\mathbb{C}}$. Up to scalar multiples, there is a unique Riemannian metric on $P(V_-)$ invariant under the action of $\mathbf{PU}(2,1)$, which turns it into a Hermitian symmetric space often denoted by $\mathbf{H}^2_{\mathbb{C}}$, and called the complex hyperbolic plane. In the present paper, we will not need a specific normalization of the metric. We mention for completeness that any invariant metric is Kähler, with holomorphic sectional curvature a negative constant (the real sectional curvatures are 1/4-pinched).

The full isometry group of $\mathbf{H}^2_{\mathbb{C}}$ is given by

$$\widehat{\mathbf{PU}(2,1)} = \langle \mathbf{PU}(2,1), \iota\rangle,$$

where ι is given in homogeneous coordinates by complex conjugation $Z \mapsto \overline{Z}$.

Still denoting (Z_1, Z_2, Z_3) the coordinates of $\mathbb{C}^3$, one easily checks that V_- can contain no vector with $Z_3 = 0$, hence we can describe its image in $\mathbf{P}^2_{\mathbb{C}}$ in terms of non-homogeneous coordinates $w_1 = Z_1/Z_3$, $w_2 = Z_2/Z_3$, where $P(V_-)$ corresponds to the Siegel half space

$$|w_1|^2 + 2\ \mathrm{Re}\ w_2 < 0.$$

The ideal boundary of complex hyperbolic space is defined as $\partial_\infty \mathbf{H}^2_{\mathbb{C}} = P(V_0)$. It is described almost entirely in the affine chart $\mathbb{Z}_3 \neq 0$ used to define the Siegel half space, only $(1,0,0)$ is sent off to infinity. We denote by p_∞ the corresponding point in $\partial_\infty \mathbf{H}^2_{\mathbb{C}}$.

The unipotent stabilizer of $(1,0,0)$ acts simply transitively on $\partial_\infty \mathbf{H}^2_{\mathbb{C}} \setminus \{p_\infty\}$, which allows to identify $\partial_\infty \mathbf{H}^2_{\mathbb{C}}$ with the one-point compactification of the Heisenberg group $\mathfrak{N}$.

Here recall that $\mathfrak{N}$ is defined as $\mathbb{C} \times \mathbb{R}$ equipped with the following group law

$$(z,t) \cdot (z',t') = (z+z', t+t'+2\mathrm{Im}(z\overline{z}')).$$

Any point $p = (z,t) \in \mathfrak{N}$ has the following lift to $\mathbb{C}^{2,1}$:

$$\tilde{p} = \begin{bmatrix} (-|z|^2 + it)/2 \\ z \\ 1 \end{bmatrix}$$

while p_∞ lifts to $(1,0,0)$.

It is a standard fact that the above form can be diagonalized, say by using the change of homogeneous coordinates given by $U_2 = Z_2$, $U_1 = (Z_1 + Z_3)/\sqrt{2}$, $U_3 = (Z_1 - Z_3)/\sqrt{2}$. With these coordinates, the Hermitian form reads

$$\langle U, V \rangle = U_1 \overline{V}_1 + U_2 \overline{V}_2 - U_3 \overline{V}_3,$$

and in the affine chart $U_3 \neq 0$, with coordinates $u_1 = U_1/U3$, $u_2 = U_2/U_3$, $\mathbf{H}^2_{\mathbb{C}}$ corresponds to the unit ball $\mathcal{B}^2 \subset \mathbb{C}^2$, given by

$$|u_1|^2 + |u_2|^2 < 1.$$

In this model the ideal boundary is simply given by the unit sphere $S^3 \subset \mathbb{C}^2$. This gives $\partial_\infty \mathbf{H}^2_{\mathbb{C}}$ a natural CR-structure (see the introduction and the references given there).

We will use the classification of isometries of negatively curved spaces into elliptic, parabolic and loxodromic elements, as well as a slight algebraic refinement; an elliptic isometry is called **regular elliptic** is its matrix representatives have distinct eigenvalues.

Non-regular elliptic elements in $\mathbf{PU}(2,1)$ fix a projective line in $\mathbf{P}^2_{\mathbb{C}}$, hence they come into two classes, depending on the position of that line with respect to $\mathbf{H}^2_{\mathbb{C}}$. If the projective line intersects $\mathbf{H}^2_{\mathbb{C}}$, the corresponding isometry is called a **complex reflection in a line**; if it does not intersect $\partial_\infty \mathbf{H}^2_{\mathbb{C}}$, then the isometry is called a **complex reflection in a point**. Complex reflection in points do not have any fixed points in the ideal boundary.

The only parabolic elements we will use in this paper will be **unipotent** (i.e. some matrix representative in $U(2,1)$ has 1 as its only eigenvalue).

Finally, we mention the classification of totally geodesic submanifolds in $\mathbf{H}^2_{\mathbb{C}}$. There are two kinds of totally geodesic submanifolds of real

dimension two, complex geodesics (which can be thought of copies of $\mathbf{H}^1_{\mathbb{C}}$), and totally real totally geodesic planes (copies of $\mathbf{H}^2_{\mathbb{R}}$).

In terms of the ball model, complex lines correspond to intersections with $\mathcal{B}^2$ of affine lines in $\mathbb{C}^2$. In terms of projective geometry, they are parametrized by their so-called polar vector, which is the orthogonal complement of the corresponding plane in $\mathbb{C}^3$ with respect to the Hermitian form $\langle \cdot, \cdot \rangle$.

The trace on $\partial_\infty \mathbf{H}^2_{\mathbb{C}}$ of a complex geodesic (resp. of a totally real totally geodesic plane) is called a $\mathbb{C}$-circle (resp. an $\mathbb{R}$-circle).

For completeness, we mention that there exists a unique complex line through any pair of distinct points $p, q \in \partial_\infty \mathbf{H}^2_{\mathbb{C}}$. The corresponging $\mathbb{C}$-circle is split into two arcs, but there is in general no preferred choice of an arc of $\mathbb{C}$-circle between p and q. Given p, q as above, there are infinitely many R-circles containing them. The union of all these $\mathbb{R}$-circles is called a spinal sphere (see section 2.3 for more on this).

2.2. **Generalities on Dirichlet domains.** Recall that the Dirichlet domain for $\Gamma \subset \mathbf{PU}(2,1)$ centered at $p_0 \in \mathbf{H}^2_{\mathbb{C}}$ is defined as

$$E_\Gamma = \left\{ z \in \mathbf{H}^2_{\mathbb{C}} : d(z, p_0) \leqslant d(z, \gamma p_0) \text{ for all } \gamma \in \Gamma \right\}.$$

Although this infinite set of inequalities is in general quite hard to handle, in many situations there is a finite set of inequalities that suffice to describe the same polytope (in other words, the polytope has finitely many faces).

Given a (finite) subset $S \subset \Gamma$, we denote by

$$E_S = \left\{ z \in \mathbf{H}^2_{\mathbb{C}} : d(z, p_0) \leqslant d(z, \gamma p_0) \text{ for all } \gamma \in S \right\},$$

and search for a minimal set S such that $E_\Gamma = E_S$. In particular, we shall always assume that

- $sp_0 \neq p_0$ for any $s \in S$ and
- $s_1 p_0 \neq s_2 p_0$ for any $s_1 \neq s_2 \in S$.

Indeed, $sp_0 = p_0$ would give a vacuous inequality, and $s_1 p_0 = s_2 p_0$ would give a repeated face.

Given a finite set S as above and an element $\gamma \in S$, we write $\widetilde{\gamma}$ for the bisector it defines, i.e.

$$\widetilde{\gamma} = \left\{ z \in \mathbf{H}^2_{\mathbb{C}} : d(z, p_0) = d(z, \gamma p_0) \right\}.$$

and $\widehat{\gamma}^S$ for the intersection of $\widetilde{\gamma}$ with E_S, i.e.

$$\widehat{\gamma}^S = \left\{ z \in \mathbf{H}^2_{\mathbb{C}} : d(z, p_0) = d(z, \gamma p_0),\ d(z, p_0) \leqslant d(z, sp_0)\ \forall s \neq \gamma \right\}$$

When the context is makes it clear what the set S is, we will write $\widehat{\gamma}$ for $\widehat{\gamma}^S$. We will call $\widehat{\gamma}$ a **face** of E_S when it has non empty interior in $\widetilde{\gamma}$.

The precise determination of all the faces of E_S, or equivalently the determination of a minimal set S with $E_S = E_\Gamma$ is quite difficult in general.

The main tool for proving that $E_\Gamma = E_S$ is the Poincaré polyhedron theorem, which give sufficient conditions for E_S to be a fundamental domain for the group generated by S. The assumptions are roughly as follows:

(1) S is symmetric (i.e. $\gamma^{-1} \in S$ whenever $\gamma \in S$) and the faces corresponding to γ and γ^{-1} are isometric.
(2) The images of E_S under elements in Γ give local tiling of $\mathbf{H}^2_{\mathbb{C}}$.

The conclusion of the Poincaré polyhedron theorem is then that the images of E_S under the group generated by S give a global tiling of $\mathbf{H}^2_{\mathbb{C}}$ (from this one can deduce a presentation for the group $\langle S \rangle$ generated by S).

The requirement that opposite faces be isometric justifies calling the elements of S "side pairings". We shall use a version of the Poincaré polyhedron theorem for *coset decompositions* rather than for groups, because we want to allow some elements of Γ to fix the center p_0 of the Dirichlet domain.

The statement we have in mind is stated for the simpler case of $\mathbf{H}^1_{\mathbb{C}}$ in [1], section 9.6. We assume E_S is stabilized by a certain (finite) subgroup $H \subset \Gamma$, and the goal is to show that E_S is a fundamental domain modulo the action of H, i.e. if $\gamma_1 E_S$ and $\gamma_2 E_S$ have non empty interior, then $\gamma_1 = \gamma_2 h$ for some $h \in H$.

The corresponding statement for $\mathbf{H}^2_{\mathbb{C}}$ appears in [9], with a light treatment of the assumptions that guarantee completeness, so we list the hypotheses roughly as they appear in [8]. The local tiling condition will consist of two checks, one for ridges (faces of codimension two in E_S), and one for boundary vertices. A ridge e is given by the intersection of two faces of E_S, i.e. two elements $s, t \in S$. We will call the intersection of E_S with a small tubular neighborhood of e the wedge of E_S near e.

- Given a ridge e given as the intersection of two faces corresponding to $s, t \in S$, we consider all the other ridges of E_S that are images of e under successive side pairings or elements of H, and check that the corresponding wedges tile a neighborhood of that ridge.
- Given a boundary vertex p, which is given by (at least) three elements $s, t, u \in S$, we need to consider the orbit of p in E_S using successive side pairings or elements of H, check that the corresponding images of E_S tile a neighborhood of that vertex,

and that the corresponding cycle transformations are all given by *parabolic* isometries.

The conclusion of the Poincaré theorem is that if $\gamma_1 E_S$ and $\gamma_2 E_S$ have non-empty interior, then γ_1 and γ_2 differ by right multiplication by an element of H. From this, one easily deduces a presentation for Γ, with generators given by $S \cup H$ (H can of course be replaced by any generating set for H), and relations given by ridge cycles.

2.3. **Bisector intersections.** In this section, we review some properties of bisectors and bisector intersections (see [7] or [3] for much more information on this).

Let $p_0, p_1 \in \mathbf{H}^2_{\mathbb{C}}$ be distinct points given in homogeneous coordinates by vectors $\tilde{p}_0$, $\tilde{p}_1$, chosen so that $\langle \tilde{p}_0, \tilde{p}_0 \rangle = \langle \tilde{p}_1, \tilde{p}_1 \rangle$. By definition, the **bisector** $\mathcal{B} = \mathcal{B}(p_0, p_1)$ is the locus of points equidistant of p_0, p_1. It is given in homogeneous coordinates $\mathbf{z} = (z_0, z_1, z_2)$ by the negative vectors $\mathbf{z}$ that satisfy the equation

$$|\langle \mathbf{z}, \tilde{p}_0 \rangle| = |\langle \mathbf{z}, \tilde{p}_1 \rangle|. \tag{2}$$

When $\mathbf{z}$ is not assumed to be negative, the same equation defines an **extor** in projective space. Note that $\mathbf{z}$ is a solution to this equation if and only if it is orthogonal (with respect to the indefinite Hermitian inner product) to some vector of the form $\tilde{p}_0 - \alpha \tilde{p}_1$, with $|\alpha| = 1$.

Finally, we mention that the image in projective space of the set of null vectors $\mathbf{z}$, i.e. such that $\langle \mathbf{z}, \mathbf{z}, \rangle = 0$, and that satisfy equation (2) is a sphere, which we will call either the **boundary at infinity** corresponding to the bisector, or its **spinal sphere**.

Restricting to vectors $\tilde{p}_0 - \alpha \tilde{p}_1$ which have positive square norm, we get a foliation of $\mathcal{B}(p_0, p_1)$ by complex lines given by the set of negative lines in $(\tilde{p}_0 - \alpha \tilde{p}_1)^{\perp}$ for fixed value of α. These complex lines are called the **complex slices** of the bisector Negative vectors of the from $(\tilde{p}_0 - \alpha \tilde{p}_1)$ (still with $|\alpha|$=1) parametrize a real geodesic, which is called the **real spine** of $\mathcal{B}$. The complex geodesic that it spans is called the **complex spine** of $\mathcal{B}$. There is a natural extension of the real spine to projective space, given by the non necessarily negative vectors of the form $\tilde{p}_0 - \alpha \tilde{p}_1$, we call this the **extended real spine** (the complex projective line that contains it is called the **extended complex spine**).

Geometrically, each complex slices of $\mathcal{B}$ is the preimage of a given point of the real spine under orthogonal projection onto the complex spine, and in particular, the bisector is uniquely determined by its real spine.

Given two distinct bisectors $\mathcal{B}_1$ and $\mathcal{B}_2$, their intersection is to a great extent controlled by the respective positions of their complex spines Σ_1 and Σ_2. In particular, if Σ_1 and Σ_2 intersect outside of their respective real spines, the bisectors are called **coequidistant**, and it is well known that in this case their intersection is a topological disk (often called a Giraud disk, see [3] for instance). This is an important special case of bisector intersections in the context of Dirichlet domains, since by construction all the faces are suidistant from one given point.

If the complex spines do not intersect, then they have a unique common perpendicular complex line $\mathcal{T}$. This complex line is a slice of $\mathcal{B}_1$ if and only if the real spine of Σ_1 goes through $\Sigma_1 \cap \mathcal{T}$ (and similarly for the real spine of $\mathcal{B}_2$). This gives a simple criterion to check whether bisectors with ultraparallel complex spines have a complex slice in common (this happens if the extended real spines intersect). When this happens, the bisectors are called **cotranchal**. One should beware that when this happens, the intersection can be strictly larger than the common slice (but there can be at most one complex slice in common).

The slice parameters above allow an easy parametrization of the intersection of the extors containing the bisectors, provided the bisectors do not share a slice. In this case, the intersection in projective space is a torus, where $(\alpha, \beta) \in S^1 \times S^1$ parametrizes the vector orthogonal to $\tilde{p}_0 - \alpha\tilde{p}_1$ and $\tilde{p}_2 - \beta\tilde{p}_3$. This vector can be written as

$$(\tilde{p}_0 - \alpha\tilde{p}_1) \boxtimes (\tilde{p}_2 - \beta\tilde{p}_3)$$

in terms of the Hermitian box product, see p. 43 of [7]. This can be rewritten in the form

$$V(\alpha, \beta) = c_{13} + \alpha c_{31} + \beta c_{21} + \alpha\beta c_{02}$$

where c_{jk} denotes $p_j \boxtimes p_k$.

The intersection of the bisectors (rather than the extors) is given by solving the inequality

$$||V(\alpha, \beta)||^2 < 0.$$

The corresponding equation $||V(\alpha, \beta)||^2 = 0$ is quadratic in each variable. It is known (see the analysis in [7]) that the intersection has at most two connected components. This becomes a bit simpler in the coequidistant case (then one can take $p_0 = p_2$, so that $c_{02} = 0$), where the equation is actually quadratic, rather than just quadratic in each variable.

Note that the intersection of three bisectors also has a somewhat simple implicit parametrization, namely the intersection of $\mathcal{B}_1 \cap \mathcal{B}_2$

with a third bisector $\mathcal{B}(q_1, q_2)$ has an equation

$$|\langle V(\alpha,\beta), \tilde{q}_1\rangle|^2 = |\langle V(\alpha,\beta), \tilde{q}_2\rangle|^2$$

where $\tilde{q}_j$ are lifts of q_j with the same square norm. Once again, these equations are quadratic in each variable.

Even in case the two bisectors do share a slice, one can easily locate that slice (it corresponds to an intersection point in the extended real spines), and the above parametrization is valid anywhere away from the common slice, so the singular bisector intersections can be handled with these methods as well.

We finish by mentioning that the above computations can clearly be performed either in floating point arithmetic, or with symbolic calculation software. We will use both of these in order to prove that certain bisectors intersect in a topological disk, and that some others do not intersect at all. This is perfectly valid even in floating point arithmetic. Indeed, proving that a bisector does not intersect a face amounts to proving that a certain polynomial function is strictly positive in a compact region (the compact region is obtained by taking the closure in $\mathbf{H}^2_{\mathbb{C}} \cup \partial_\infty \mathbf{H}^2_{\mathbb{C}}$). Proving that the intersection is non empty amounts to finding a point where the function is strictly negative (and then we can try to prove that the intersection is a disk because of the analysis in [7]).

A problem arises when we need to show that $||V(\alpha,\beta)||^2$ vanishes at exactly one point, which can happen for instance when the bisectors are tangent at infinity. This certainly cannot be proved by floating point arithmetic, so in these cases we will try to understand in terms of geometric arguments why there is a tangency in the picture.

The key geometric argument, that will explain all tangencies in the present paper, is the following result, proved by Phillips in [11]:

Proposition 2.1. *Let A be a unipotent isometry, and let $p_0 \in \mathbf{H}^2_{\mathbb{C}}$. Then $\mathcal{B}(p_0, Ap_0) \cap \mathcal{B}(p_0, A^{-1}p_0)$ is empty. The extension to $\partial_\infty \mathbf{H}^2_{\mathbb{C}}$ of these bisectors intersect precisely in the fixed point of A, in other words the spinal spheres for the above two bisectors are tangent at that fixed point.*

3. Boundary unipotent representations associated to the triangulation

We recall part of the results from [4], using the notation and terminology from section 1, so that M denotes the figure eight knot complement. We will interchangeably use the following two presentations for

$\pi_1(M)$:

$$\langle\ g_1, g_2, g_3 \mid g_2 = [g_3, g_1^{-1}],\ g_1 g_2 = g_2 g_3\ \rangle$$

and

$$\langle\ a, b, t \mid tat^{-1} = aba,\ tbt^{-1} = ab\ \rangle.$$

The second presentation can be obtained from the first one by setting $a = g_2$, $b = [g_2, g_3^{-1}]$ and $t = g_3$. Note that a and b generate a free group F_2, and the second presentation exhibits $\pi_1(M)$ as the mapping torus of a pseudo-Anosov element of the mapping class group of F_2; this comes from the fact that the figure eight knot complement fibers of the circle, with fiber a once punctured torus.

The three representations of $\pi_1(M)$ with unipotent boundary holonomy are the following (see [4] pages 102-105). We only give the image of g_1 and g_3, since they clearly generate the group.

$$\rho_1(g_1) = \begin{pmatrix} 1 & 1 & -\frac{1}{2} - \frac{\sqrt{3}}{2}i \\ 0 & 1 & -1 \\ 0 & 0 & 1 \end{pmatrix}, \quad \rho_1(g_3) = \begin{pmatrix} 1 & 0 & 0 \\ 1 & 1 & 0 \\ -\frac{1}{2} - \frac{\sqrt{3}}{2}i & -1 & 1 \end{pmatrix}.$$

$$\rho_2(g_1) = \begin{pmatrix} 1 & 1 & -\frac{1}{2} - \frac{\sqrt{7}}{2}i \\ 0 & 1 & -1 \\ 0 & 0 & 1 \end{pmatrix}, \quad \rho_2(g_3) = \begin{pmatrix} 1 & 0 & 0 \\ -1 & 1 & 0 \\ -\frac{1}{2} + \frac{\sqrt{7}}{2}i & 1 & 1 \end{pmatrix}.$$

$$\rho_3(g_1) = \begin{pmatrix} 1 & 1 & -1/2 \\ 0 & 1 & -1 \\ 0 & 0 & 1 \end{pmatrix}, \quad \rho_3(g_3) = \begin{pmatrix} 1 & 0 & 0 \\ \frac{5}{4} - \frac{\sqrt{7}}{4}i & 1 & 0 \\ -1 & -\frac{5}{4} - \frac{\sqrt{7}}{4}i & 1 \end{pmatrix}.$$

From this point on, we mainly focus on the representation ρ_2, and write

$$G_1 = \rho_2(g_1), \quad G_2 = \rho_2(g_2), \quad G_3 = \rho_2(g_3).$$

For completeness, we state the following result (which is almost proved in [4]).

Proposition 3.1. *For any irreducible representation $\rho : \pi_1(M) \to \mathbf{PU}(2,1)$ with unipotent boundary holonomy, ρ (or $\overline{\rho}$) is conjugate to ρ_1, ρ_2 or ρ_3.*

Proof: We follow the begining of section 5.4 in [4]. To prove that we have all representations we only need to complete the argument there to exclude degenerate cases.

We first observe that one of the boundary holonomy generators is given by ${g_1}^{-1} g_2 = {g_1}^{-1} g_3 {g_1}^{-1} {g_3}^{-1} g_1$. This is conjugate to ${g_1}^{-1}$ so $G_1 = \rho(g_1)$ is unipotent by assumption. Moreover, g_1 is conjugate to g_3, which implies that $G_3 = \rho(g_3)$ is unipotent as well.

We suppose the representation is not the identity representation. Let p_1 and p_2 be the parabolic fixed points of $G_1 = \rho(g_1)$ and $G_2 = \rho(g_2)$, respectively. We may assume that $p_1 \neq p_2$ otherwise the representation is elementary.

Define $q_1 = {G_1}^{-1}(p_2)$ and $q_3 = G_3(p_1)$. By Lemma 5.3 in [4],

$$G_3{G_1}^{-1}(p_2) = {G_1}^{-1}G_3(p_1).$$

We define $q_2 = G_3{G_1}^{-1}(p_2) = {G_1}^{-1}G_3(p_1)$ as that point.

If p_1, p_2, q_1, q_2 and p_1, p_2, q_2, q_3 are in general position (that is, no three points belong to the same complex line) these tetrahedra are indeed parametrized by the coordinates from [4], and we obtain the side pairings of the two tetrahedra p_1, p_2, q_1, q_2 and p_1, p_2, q_2, q_3 leading to the above representations.

If the points are not in general position we analyze the representation case by case.

The first case is when $q_1 = {G_1}^{-1}(p_2)$ belongs to the boundary of the complex line through p_1 and p_2. Without loss of generality, we may assume $p_1 = \infty$ and $p_2 = (0, 0)$ in Heisenberg coordinates. As G_1 preserves the complex line between p_1 and p_2 it has the following form:

$$G_1 = \begin{pmatrix} 1 & 0 & \frac{it}{2} \\ 0 & 1 & 0 \\ 0 & 0 & 1 \end{pmatrix}.$$

We then write

$$G_3 = \begin{pmatrix} 1 & 0 & 0 \\ z & 1 & 0 \\ -\frac{|z|^2}{2} + \frac{is}{2} & -\bar{z} & 1 \end{pmatrix}.$$

with $z \neq 0$ (otherwise the group is reducible). Now, the equation

$${G_3}^{-1}{G_1}^{-1}(p_2) = {G_1}^{-1}G_3(p_1)$$

gives

$$\begin{pmatrix} -\frac{it}{2} \\ -\frac{i\bar{z}t}{2} \\ \frac{it|z|^2}{4} + \frac{ts}{4} + 1 \end{pmatrix} = \lambda \begin{pmatrix} \frac{it|z|^2}{4} + \frac{ts}{4} + 1 \\ z \\ -\frac{|z|^2}{2} + \frac{is}{4} \end{pmatrix}.$$

One easily checks that this equation has no solutions with $z \neq 0$. Therefore p_3 is not in the complex line defined by p_1 and p_2. Analogously, $q_3 = G_3(p_1)$ cannot be in that complex line either. Now, from the side pairings we obtain that p_1, q_1, q_2 and p_2, q_2, q_3 are in general position. It remains to verify that p_2, q_1, q_2 are in general position. We write

$$(p_2, q_1, q_2) = (p_2, {G_1}^{-1}(p_2), {G_1}^{-1}G_3(p_1)) = {G_1}^{-1}G_3({G_3}^{-1}G_1(p_2), p_2, p_1)$$

But if $({G_3}^{-1}G_1(p_2), p_2, p_1)$ are on the same complex line then, again, we obtain equations which force p_1, p_2, q_1 to be in the same line. □

In fact it is not hard to show that there are no reducible representations except elementary ones (still with unipotent boundary holonomy). Finally, these elementary representations, by using the relator relation, satisfy $\rho(g_1) = \rho(g_3)$.

4. A Dirichlet domain for Γ

The combinatorics of Dirichlet domains depend significantly on their center p_0, and there is of course no canonical way to choose this center. We will choose a center that produces a Dirichlet domain with very few faces, and that has a lot of symmetry (see section 4.1).

Recall that Γ denotes $\Gamma_2 = \rho_2(\pi_1(M))$, and G_k denotes $\rho_2(g_k)$, see section 3. Recall that $G_2 = [G_3, G_1^{-1}]$, and this can easily be computed to be

$$G_2 = \begin{pmatrix} 2 & \frac{3}{2} - i\frac{\sqrt{7}}{2} & -1 \\ -\frac{3}{2} - i\frac{\sqrt{7}}{2} & -1 & 0 \\ -1 & 0 & 0 \end{pmatrix}$$

It is easy to check that G_2 is a regular elliptic element of order 4, whose isolated fixed point is given in homogeneous coordinates by

$$\tilde{p}_0 = (2, -(3 + i\sqrt{7})/2, -2).$$

Note also that no power of G_2 fixes any point in $\partial_\infty \mathbf{H}^2_{\mathbb{C}}$ (G_2 and G_2^{-1} are regular elliptic, and G_2^2 is a complex reflection in a point).

As in section 2.2, E_Γ denotes the Dirichlet domain centered at p_0, and E_S denotes an a priori larger domain taking into account only the faces coming from S rather than all of Γ.

From this point on, we will always fix the set S to be the following set of eight group elements:

$$S = \{G_2^k G_1 G_2^{-k}, G_2^k G_3^{-1} G_2^{-k}, k = 0, \dots, 3\}. \tag{3}$$

Since for the remainder of the paper we will always use the same set S, we will set

$$E = E_S,$$

in order to make the notation lighter.

With this notation, what we intend to prove is that $E = E_\Gamma$, which is equivalent to saying that E_Γ has precisely eight faces, given by the eight elements in S, see equation (3). For future reference, we state this as follows:

Proposition 4.1. *The Dirichlet domain has precisely eight faces, given by the orbit of p_0 under G_1, G_3^{-1} as well as their conjugates under powers of G_2.*

Note that E is not a fundamental domain for Γ, since by construction it has a nontrivial stabilizer (powers of G_2 fix the center of E, hence they must preserve E). It is a fundamental domain for the coset decomposition of Γ into left cosets of the group H of order 4 generated by G_2 (see section 2.2), and this suffices to produce a presentation for Γ, see section 5.3. One can deduce from E a fundamental domain for Γ, by taking $E \cap F$ where F is any fundamental domain for H. We omit the details of that construction, since they will not be needed in the what follows.

As already mentioned in section 2.2, in order to prove that $E_\Gamma = E$, we will start by determining the precise combinatorics of E, then apply the Poincaré polyhedron theorem in order to prove that E is a fundamental domain for Γ modulo the action of the finite group H.

We order the faces as in Table 1, in order to make the intersection pattern of faces as simple as possible.

Index	Element of S	Bisector	Face
#1	G_1	$\mathcal{B}$	b
#2	G_3^{-1}	$\mathcal{B}^-$	b^-
#3	$G_2G_1G_2^{-1}$	$G_2\mathcal{B}$	G_2b
#4	$G_2G_3^{-1}G_2^{-1} = G_1^{-1}$	$G_2\mathcal{B}^-$	G_2b^-
#5	$G_2^2G_1G_2^2 = G_2^{-1}G_3G_2$	$G_2^2\mathcal{B}$	G_2^2b
#6	$G_2^2G_3^{-1}G_2^2 = G_2G_1^{-1}G_2^{-1}$	$G_2^2\mathcal{B}^-$	$G_2^2b^-$
#7	$G_2^{-1}G_1G_2 = G_3$	$G_2^{-1}\mathcal{B}$	$G_2^{-1}b$
#8	$G_2^{-1}G_3^{-1}G_2$	$G_2^{-1}\mathcal{B}^-$	$G_2^{-1}b^-$

TABLE 1. Notation for the eight faces of the Dirichlet domain. The equalities in the second column follow from the relation $G_1G_2 = G_2G_3$.

4.1. **Symmetry.** Note that S is by construction invariant under conjugation by G_2, which fixes p_0, so E is of course G_2-invariant. In particular, it has at most 2 isometry types of faces; in fact all its faces are isometric, as can be seen using the involution

$$I = \begin{pmatrix} 0 & 0 & 1 \\ 0 & -1 & 0 \\ 1 & 0 & 0 \end{pmatrix}.$$

This is not an element of Γ, but it can easily be checked that it normalizes Γ by using the conjugacy information given in Proposition 4.2.

Proposition 4.2.

$$IG_1I = G_3^{-1}$$

$$IG_2I = G_2^{-1}$$

This proposition shows that the group generated by I and G_2 has order 8, and this group of order 8 stabilizes E (the formula given above for p_0 makes it clear that it is fixed by I). Finally, note that Proposition 4.2 makes it clear that I exchanges the faces b and b^-.

4.2. **Vertices of E.** In this section we describe certain fixed points of unipotent elements in the group, which will turn out to give the list of all vertices of E (this claim will be proved justified in the end of section 4.3, see Proposition 4.6). We use the numbering of faces (as well as bisectors that contain these faces) given in 1. We start mentioning that G_1 clearly maps $\mathcal{B}(p_0, G_1^{-1}p_0)$ to $\mathcal{B}(p_0, G_1p_0)$, i.e. bisector #1 to #4. Since G_1 is unipotent, Proposition 2.1 shows that the corresponding bisectors have empty intersection, and their spinal spheres are tangent at the fixed point of G_1.

The latter is clearly given by

$$p_1 = (1, 0, 0),$$

and it is easy to check that this point is on precisely four bisectors from the Dirichlet domain, namely #1,2,3 and 4. The fact that it is on faces #1 and #4 is obvious, the other ones can be checked by explicit computation. Indeed, we have

$$G_3p_1 = (1, -1, \frac{-1 + i\sqrt{7}}{2}),$$

$$G_1^{-1}G_2^{-1}p_1 = (\frac{1 - i\sqrt{7}}{2}, -1, -1)$$

hence

$$|\langle p_1, G_3^{-1}p_0\rangle| = |\langle G_3p_1, p_0\rangle| = 2 = |\langle p_1, p_0\rangle|$$

$$|\langle p_1, G_2G_1G_2^{-1}p_0\rangle| = |\langle G_1^{-1}G_2^{-1}p_1, p_0\rangle| = 2 = |\langle p_1, p_0\rangle|.$$

Similarly, faces #2 and #5 have tangent spinal spheres, and this comes from the fact that $G_2^{-1}G_3$ is unipotent (which can be checked by direct calculation). Indeed, this isometry sends $\mathcal{B}^- = \mathcal{B}(p_0, G_3^{-1}p_0)$ to $\mathcal{B}(G_2^{-1}G_3p_0, G_2^{-1}p_0) = \mathcal{B}(G_2^{-1}G_3G_2p_0, p_0)$.

We call q_1 the fixed point of $G_2^{-1}G_3$, which can easily be computed to be given by

$$q_1 = (\frac{-1+i\sqrt{7}}{2}, 1, 1).$$

One easily verifies that this point is on (the boundary of) precisely four faces of the Dirichlet domain, namely #2,3,4,5.

Now applying G_2 to both p_1 and q_1, we get eight specific fixed points of unipotents in the group which are all tangency points of certain spinal spheres. Perhaps surprisingly, the eight tangency points will turn out to give all the vertices of the Dirichlet domain. We summarize the results in the following.

Proposition 4.3. *There are precisely eight pairs of tangent spinal spheres among the boundary at infinity of the faces of the Dirichlet domain. The list of points of tangency is given in Table 2.*

Vertex	*old name*	*Fixed by*	*Tangent spinal spheres*	*Other faces*
p_1	(v_0)	G_1	*#1, #4*	*#2, #3*
p_2	(v_1)	G_3	*#7, #2*	*#8, #1*
p_3	(v_7)	$G_2^{-1}G_3G_2$	*#5, #8*	*#6, #7*
p_4	(v_5)	$G_2G_1G_2^{-1}$	*#3, #6*	*#4, #5*
q_1	(v_6)	$G_3^{-1}G_2$	*#2, #5*	*#3, #4*
q_2	(v_4)	$G_1^{-1}G_2$	*#4, #7*	*#5, #6*
q_3	(v_3)	$G_2G_1^{-1}$	*#6, #1*	*#7, #8*
q_4	(v_2)	G_3G_1	*#8, #3*	*#1, #2*

TABLE 2. The vertices of E at infinity, given by a unipotent element that fixes them.

Proof: The claim about tangency has already been proved, we only justify the fact that the points in the orbit of p_1 and q_1 are indeed stabilized by the unipotent element given in Table 2. This amounts to checking that the unipotent elements fixing the points p_j (resp. those fixing the points q_j) are indeed conjugates of each other under powers of G_2.

This can easily be seen from the presentation of the group (in fact the relations $G_1G_2 = G_2G_3$ and $(G_1G_2)^3 = 1$ suffice to check this). For instance, $G_2(p_4) = p_3$ because, using standard word notation in the generators where $1 = G_1$, we have $\overline{1} = G_1^{-1}$.

$$2 \cdot 2\overline{1}\,\overline{2} \cdot \overline{2} = 222121\overline{2} = \overline{2}231\overline{2} = 323\overline{2}\,\overline{2} = 32322 = \overline{2}\,\overline{3}2.$$

Similarly, $G_2(q_3) = q_4$ because

$$2 \cdot 2\overline{1} \cdot \overline{2} = 222121 = \overline{2}231 = 31.$$

The other conjugacies are handled in a similar fashion. □

4.3. **Combinatorics of E.** We now go into the detailed study of the combinatorics of E. The observations from section 4.1 show that it is enough to determine the combinatorics of one single face, say $\mathcal{B}$, and its incidence relation to all other faces.

We denote by $b = \mathcal{B} \cap E$, and by $\overline{b}$ the closure of that face in $\mathbf{H}^2_{\mathbb{C}} \cup \partial_\infty \mathbf{H}^2_{\mathbb{C}}$. The combinatorics of $\overline{b}$ are depicted in Figure 2, where the shaded region corresponds to the 2-face of $\overline{b}$ at infinity (i.e the intersection of the face with the spinal sphere bounding $\mathcal{B}$). There are two other 2-faces, both of which are Giraud disks, given by

$$G_2^{-1}\overline{\mathcal{B}^-} \cap \overline{\mathcal{B}} \text{ and } \overline{\mathcal{B}} \cap \overline{\mathcal{B}^-},$$

and we claim that the intersection with all faces other than $G_2^{-1}\overline{\mathcal{B}^-}$ and $\overline{\mathcal{B}^-}$ occur in lower-dimension.

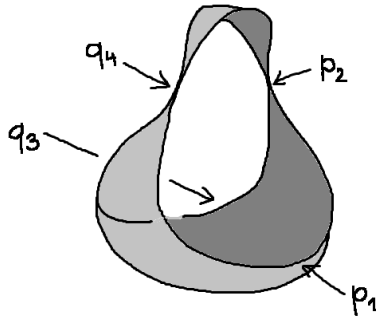

FIGURE 2. Face $\mathcal{B}$ has four vertices, indicated on the figure (they are the fixed points of G_1, G_3, G_3G_1, and $G_1G_2^{-1}$).

The general remark is that these claims can be proved using the techniques from section 2.3. For completeness, we expand a little on these verifications.

Since all eight bisectors bounding E are coequidistant, their pairwise intersections are either empty, or diffeomorphic to a disk (see section 2.3). Recall that such disks are either complex lines, or Giraud disks.

Proposition 4.4 gives intersections of $\mathcal{B}$ with all other seven bisectors. It can easily be translated into a statement about $\mathcal{B}^-$ by using the involution I (see section 4.1).

Proposition 4.4. *$\mathcal{B}$ intersects exactly four of the seven other bisectors bounding E, namely $G_2^{-1}\mathcal{B}$, $G_2^{-1}\mathcal{B}^-$, $\mathcal{B}^-$, and $G_2\mathcal{B}$. The corresponding intersections are Giraud disks.*

Proof:

The fact that the intersection of $\mathcal{B}$ with the other four bisectors in the statement is indeed a Giraud disk, as well as $\mathcal{B} \cap G_2^2\mathcal{B} = \emptyset$ can be shown with computer calculations (see section 2.3). The fact that $\mathcal{B} \cap G_2\mathcal{B}^-$ and $\mathcal{B} \cap G_2^2\mathcal{B}^-$ are empty follows from Proposition 4.3. □

We now give a statement analogous to Proposition 4.4, pertaining to face (rather than bisector) intersections.

Proposition 4.5. (1) *$\mathcal{B} \cap G_2^{-1}\mathcal{B} \cap E$ and $\mathcal{B} \cap G_2\mathcal{B} \cap E$ are empty.*
(2) *$\mathcal{B} \cap \mathcal{B}^- \cap E = \mathcal{B} \cap \mathcal{B}^-$ and $\mathcal{B} \cap G_2^{-1}\mathcal{B}^- \cap E = \mathcal{B} \cap G_2^{-1}\mathcal{B}^-$ are Giraud disks.*

Proof: In order to prove this, we will use spinal coordinates on the relevant Giraud disks (i.e. the ones that appear in Proposition 4.5), and for each of them we plot the trace on that Giraud disk of the other six bisectors (see section 2.3 for a description of how this can be done).

The results are shown for $\mathcal{B} \cap G_2^{-1}\mathcal{B}$ and $\mathcal{B} \cap \mathcal{B}^-$ in Figure 3, where we have labelled each arc with the index of the corresponding bisector according to the numbering in Table 1. Note that these curves were all

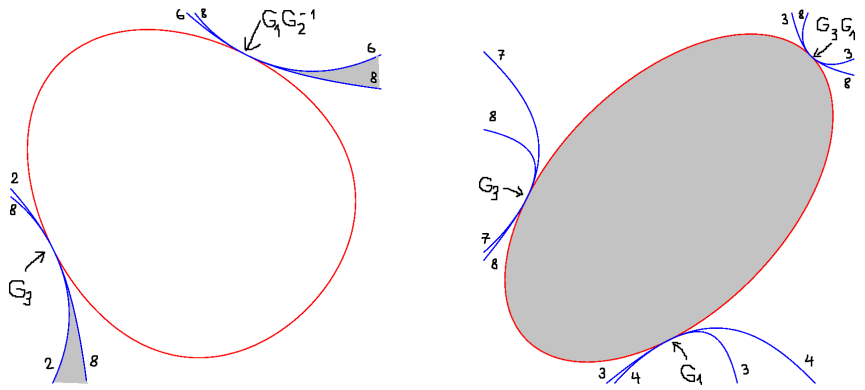

(a) $\mathcal{B} \cap G_2^{-1}(\mathcal{B})$ (b) $\mathcal{B} \cap \mathcal{B}^-$

FIGURE 3. Typical Giraud disk corresponding to the intersection of two bounding bisectors; the other curves are traces of the other 6 bisectors.

drawn using the 'implicitplot' command Maple, hence they should be taken with a grain of salt - they do however prove the combinatorics of verious face intersections provided we are able to prove that

- the curves that look tangent on the picture really are tangent and
- the bisectors not appearing in the picture really do not intersect the corresponding Giraud torus.

The second part is easy (see the discussion at the end of section 2.3). The first one follows from the analysis of tangencies of spinal spheres given in 4.3. The triple intersections that we need to analyze in order to justify correctness of Figure 3(a) are the following:

$$1, 6, 7; \quad 1, 7, 8; \quad 1, 2, 7$$

The first and third case are obvious, since the bisectors 1 and 6 (resp. 2 and 7) have tangent spinal spheres (see Proposition 4.3). In order to analyze $1, 7, 8$, we distinguish two cases, corresponding to the tangency at the fixed point of $G_1 G_2^{-1}$ and at the fixed point of G_3.

We only work with G_3, the other case is entirely similar. The point is that we know the fixed point of G_3 lies on (the closures of) four faces, numbered $1, 2, 7, 8$. Since the spinal spheres for 3 and 8 are tangent, the curve for $1, 7, 8$ is tangent to that for $1, 2, 7$, which proves the claim. □

It follows from the previous analysis that the face b has no vertex in $\mathbf{H}^2_{\mathbb{C}}$, and that it has exactly four ideal vertices, or in other words the closure $\overline{b}$ has four vertices. We summarize this in the following proposition:

Proposition 4.6. *$\overline{b}$ has precisely four vertices, all at infinity. They are given by p_1, p_2, q_3, q_4.*

One can easily use symmetry to give the list of vertices of every face. Each face has precisely four (ideal) vertices.

Proof: p_2 and q_3 are obtained as the only two points in the intersection $\overline{\mathcal{B}} \cap G_2^{-1}\overline{\mathcal{B}}$ (bars denote the closures in $\mathbf{H}^2_{\mathbb{C}} \cup \partial_\infty \mathbf{H}^2_{\mathbb{C}}$), see Figure 3. Similarly, p_1 and q_4 are the two points in $\overline{\mathcal{B}} \cap G_2 \overline{\mathcal{B}}$. □

5. The Poincaré polyhedron theorem for E

This section is devoted to proving the hypotheses of the Poincaré polyhedron theorem for the Dirichlet polyhedron E (sections 5.1 and 5.2), and to state some straightforward applications (section 5.3).

5.1. **Ridge cycles.** It follows from Giraud's theorem that the ridges of E are on precisely three bisectors, hence there will be three copies of E tiling a its neighborhood. We only need to consider the ridges $b \cap b^-$

and $b \cap G_2^{-1}(b^-)$, since the other ones are all images of these two under the appropriate power of G_2.

The Giraud disk $\mathcal{B} \cap \mathcal{B}^-$ is equidistant of p_0, $G_1(p_0)$ and $G_3^{-1}(p_0)$, and we apply G_1^{-1} to this triple of points, getting $G_1^{-1}p_0, p_0, G_1^{-1}G_3^{-1}p_0 = G_2G_1p_0$, and bring it back to $\mathcal{B} \cap \mathcal{B}^-$ by applying G_2^{-1}. This does not yield the identity, but effects a cyclic permutation of the above three points:

$$\begin{array}{c} p_0, G_1p_0, G_3^{-1}p_0 \\ \downarrow G_2 \\ G^{-1}p_0, p_0, G_1^{-1}G_3^{-1}p_0 \\ \downarrow G_1 \\ G_3^{-1}p_0, p_0, G_1p_0 \end{array}$$

In other words, the corresponding cycle transformation is G_1G_2, and the corresponding relation is

$$(G_1G_2)^3 = I.$$

The Giraud disk $\mathcal{B} \cap G_2^{-1}(\mathcal{B}^-)$ is equidistant of p_0, $G_1(p_0)$ and $G_3G_1(p_0)$. Again, we get an isometry in the group that permutes these points cyclically:

$$\begin{array}{c} p_0, G_1p_0, G_3G_1p_0 \\ \downarrow G_2^2 \\ G_1^{-1}p_0, p_0, G_1^{-1}G_3G_1p_0 \\ \downarrow G_1 \\ G_3G_1p_0, p_0, G_1p_0 \end{array}$$

which gives the relation

$$(G_1G_2^2)^3 = I.$$

5.2. **Cycles of boundary vertices.** As explained in section 2.2, we need to check that the cycle transformations for all boundary vertices are parabolic. There only one cycle of vertices, since $G_2(q_k) = q_{k+1}$, $G_2(p_k) = p_{k-1}$ (indices mod 4), and we have

$$G_3(p_1) = q_3.$$

We check the geometry of the tiling of $\mathbf{H}^2_{\mathbb{C}}$ near p_1, which can be deduced from the structure of ridges through that point (see section 5.1). Recall that p_1 is on four faces, namely #1, 2, 3 and 4 (see section 4.3). We look at the relevant ridges, and examine the local tiling around $(1, 2)$, $(2, 3)$ and $(3, 4)$. Note that $(3, 4)$ is just the image of $(1, 2)$ under G_2, and $(2, 3)$ is the image of $(8, 1)$ under G_2. The results are summarized in Table 3. The images of E that appear only once are indicated in bold, namely they are $G_1^{-1}(E)$ and $G_1(E)$, and their interfaces with E are identified by G_1, which is of course parabolic.

Ridge	Local tiling
$1, 2$	$E, \mathbf{G_1}(\mathbf{E}), G_2^{-1}G_1^{-1}(E) = G_3^{-1}(E)$
$2, 3$	$E, G_2G_1(E), G_3^{-1}(E)$
$3, 4$	$E, G_2G_1(E), \mathbf{G_1^{-1}}(\mathbf{E})$

TABLE 3. Local tilings for ridges meeting in the fixed point of G_1.

Now that we have checked cycles of ridges and boundary vertices, the Poincaré polyhedron theorem shows that E is a fundamental domain for the action of Γ modulo the action of G_2 (the latter isometry generates the stabilizer of the center p_0 in Γ). The main consequences will be drawn in section 5.3.

We state above result about cycles of boundary vertices in a slightly stronger form.

Proposition 5.1. *The stabilizer of p_1 in Γ is the cyclic group generated by G_1. The stabilizer of q_1 is generated by $G_2^{-1}G_3$.*

The proposition follows from the above analysis (taking further care of the corresponding orbits of vertices). We give a slightly different proof, using the Poincaré polyhedron theorem (in other words using the fact that the images of E under elements of Γ tile $\mathbf{H}^2_{\mathbb{C}}$).

Proof: Since each vertex of E is on four faces, it must be sent to some vertex of E by at least (in fact precisely) four side-pairings from the list in Table 1. These orbit relations are given in Figure 4, where we have used the side-pairings from Table 1, the fact that we know some elements in the stabilizer of each vertex (see Table 2), and the G_2-orbit relations between the p_j and q_k.

Clearly the fundamental group of the graph (based say at the vertex labelled p_1), has a natural representation into Γ induced by the labelling. Concretely, each loop in the graph gives an element of Γ in the obvious way, by taking the product of the labels in the appropriate order (we take the inverse of the label when going along the oriented edge backwards).

The Poincaré polyhedron implies that the stabilizer of p_1 is in fact the image of the above representation, which may seem a bit hard to describe given the complexity of the graph. In fact it is not too hard to simplify this graph by using the presentation of the group Γ (in order to do this, we do not need to know that we have a full set of relations, it is enough to know that the relations from the presentation holds, which can be checked by direct computations).

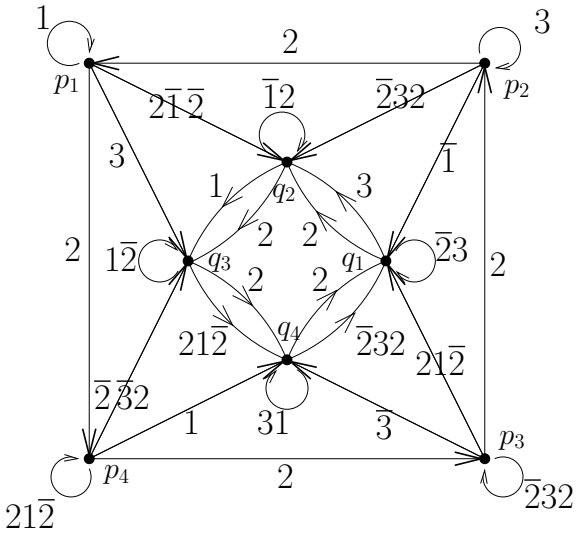

FIGURE 4.

Using the relations in the presentation, it is not hard to produce simpler and simpler graphs that yield the same stabilizer, as indicated in Figures 5-7 (on the side of each picture, we give quick justifications when the simplification is not obvious).

□

5.3. **Presentation.** The Poincaré polyhedron theorem (see section 2.2) gives the following presentation

$$\langle G_1, G_2 | G_2^4, (G_1G_2)^3, (G_1G_2^2)^3 \rangle$$

or in other words, since $G_1G_2 = G_2G_3$,

$$\langle G_2, G_3 | G_2^4, (G_2G_3)^3, (G_2G_3G_2)^3 \rangle.$$

It also gives precise information about the elliptic elements in the group.

Proposition 5.2. *Let $\gamma \in \Gamma$ be a non trivial torsion element. Then γ has no fixed point in $\partial_\infty \mathbf{H}^2_{\mathbb{C}}$.*

Proof: It follows from the Poincaré polyhedron theorem that any elliptic element in Γ must be conjugate to some power of a cycle transformation of some cell in the skeleton of the fundamental domain. This says that any elliptic element in the group must be conjugate to a power of G_2 (which fixes the center of the Dirichlet domain), or G_1G_2 (which fixes the ridge which is the intersection of faces $b \cap b^-$) or $G_1G_2^2$

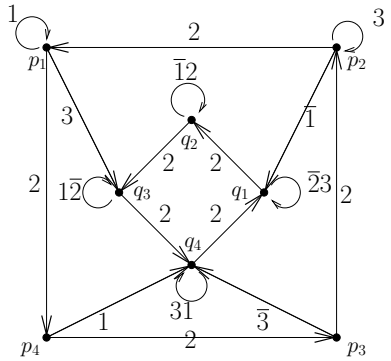

$$p_1 \overset{2\overline{1}\,\overline{2}}{\to} q_2: \quad \overline{2}31 = \overline{2}\,\overline{2}121 = 22121 = 2\overline{1}\,\overline{2}$$

$$p_2 \overset{\overline{2}32}{\to} q_2: \quad 2\overline{1}3 = 22\overline{3}\,\overline{2}\,\overline{3} = \overline{2}32$$

$$p_4 \overset{\overline{2}\,\overline{3}2}{\to} q_3: \quad \overline{2}\,\overline{3}2 = \overline{2}\,\overline{2}\,\overline{1}22 = 22\overline{1}22$$

$$p_3 \overset{21\overline{2}}{\to} q_1: \quad 21\overline{2} = 22322$$

$$p_2 \overset{2}{\to} p_2: \quad 3 = \overline{2}12$$

FIGURE 5. First stage of simplification of the orbit graph; when it is not obvious, we justify why the edges can be removed.

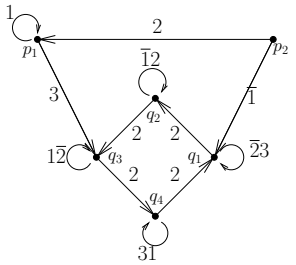

$$p_1 \overset{2}{\to} p_4: \quad \overline{1}23 = \overline{1}12 = 2$$

$$p_3 \overset{2}{\to} p_2: \quad 12\overline{3} = 23\overline{3} = 2$$

$$q_4 \overset{1}{\leftarrow} p_4 \overset{2}{\to} p_3 \overset{\overline{3}}{\to} q_4: \quad \overline{3}2\overline{1} = \overline{2}\,\overline{1}\,\overline{2}\,\overline{2}\,\overline{1} = 21221\overline{2}\,\overline{1} = 2232 = 222 \cdot \overline{2}3 \cdot 2$$

FIGURE 6. Second stage of simplification.

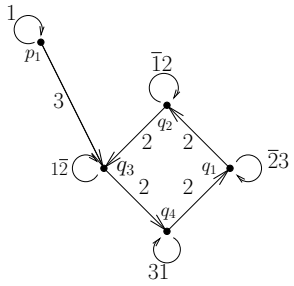

$$p_1 \overset{2}{\leftarrow} p_2 \overset{\overline{1}}{\rightarrow} q_1 : \quad \overline{1}\,\overline{3}22\overline{1} = \overline{1}\,\overline{3}\,\overline{2}\,\overline{2}\,\overline{1} = \overline{1}\,\overline{2}\,\overline{1}\,\overline{2}\,\overline{1} = 2$$

FIGURE 7. Third stage of simplification - from this stage it is easy to reduce the graph to one single loop labelled 1, based at p_1.

(which fixes the ridge which is the intersection of faces $b \cap G_2^{-1}b^-$), see section 5.1.

G_1G_2 and $G_1G_2^2$ are regular elliptic of order three, so they no power fixes any point in $\partial_\infty \mathbf{H}^2_{\mathbb{C}}$. As for G_2, the only non regular elliptic power is G_2^2, but this can easily be checked to be a reflection in a point, so it is conjugate in $Aut(\mathcal{B}^2)$ to $(z_1, z_2) \mapsto (-z_1, -z_2)$, which has no fixed point in the unit sphere. □

Proposition 5.3. *The kernel of ρ_2 is generated as a normal subgroup by a^4, $(at)^3$ and $(ata)^3$.*

Proof: The fact that the three elements in the statement of the proposition are indeed in the kernel follows from the presentation and the fact that

$$\rho_2(a) = G_2$$
$$\rho_2(b) = G_1^{-1}G_3$$
$$\rho_2(t) = G_3.$$

We now consider the presentation

$$\langle a, b, t | tat^{-1} = aba, tbt^{-1} = ab, a^4, (at)^3, (ata)^3 \rangle.$$

One can easily get rid of the generator b, since

$$b = a^{-1}tat^{-1}a^{-1},$$

and the other relation involving b then follows from the other three relations. Indeed, one easily sees that $(at)^3 = (ata)^3 = 1$ implies $(tat)^3 = 1$, and then

$t(\mathbf{a^{-1}tat^{-1}a^{-1}})t^{-1} = ta^{-1}ta(tat)^2 = ta^{-1}(ta)^2t^2at = ta^{-1} \cdot a^{-1}t^{-1} \cdot t^2at$

$$= ta^2tat = tat^{-1}a^{-1} = a(\mathbf{a^{-1}tat^{-1}a^{-1}}).$$

In other words, the quotient group is precisely

$$\langle a, t | a^4, (at)^3, (ata)^3 \rangle,$$

which is the same as the image of ρ_2. □

6. Combinatorics at infinity of the Dirichlet domain

The next goal is to study the manifold at infinity, i.e. the quotient of the domain of discontinuity under the action of the group. The idea is to consider the intersection with $\partial\mathbf{H}^2_{\mathbb{C}}$ of a fundamental domain for the action on $\mathbf{H}^2_{\mathbb{C}}$. Recall that we did not quite construct a fundamental domain in $\mathbf{H}^2_{\mathbb{C}}$, but a fundamental domain modulo the action of a cyclic group of order 4 (generated by G_2).

We start by describing the combinatorial structure of $U = \partial_\infty E$, which is bounded by eight (pairwise isometric) pieces of spinal spheres. We picture the boundary ∂U of U in $\partial\mathbf{H}^2_{\mathbb{C}}$ in Figure 8 (this can easily be obtained from the results in section 4.3). Note that it is clear from this picture that ∂U is a torus, and the fact that it is embedded in $\partial\mathbf{H}^2_{\mathbb{C}}$ follows from the analysis of the combinatorics of E given in the previous sections.

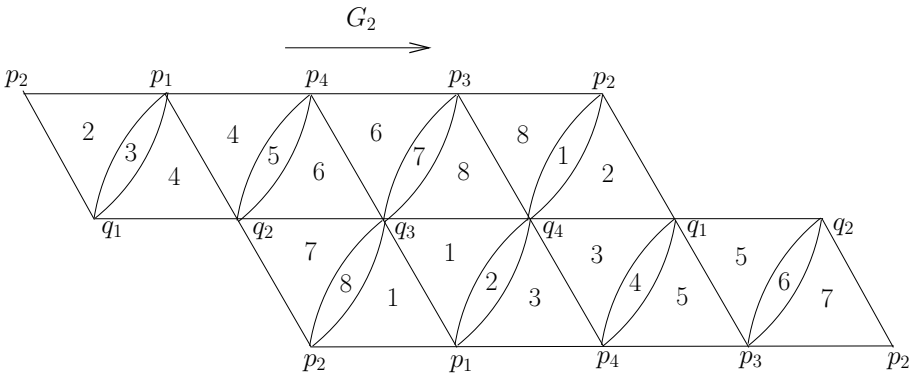

FIGURE 8. The combinatorics of $\partial_\infty E$, which is a torus. We have split each quadrilateral components of the boundary faces into two triangles along an arc of $\mathbb{C}$-circle.

Picture 9 makes it quite clear that U is a solid torus, but we justify this in detail. What we are after is an essential disk in U whose boundary is the curve on the left and right side of Figure 8. Since that curve has three sides, we will call this disk a triangle, and denote it by T.

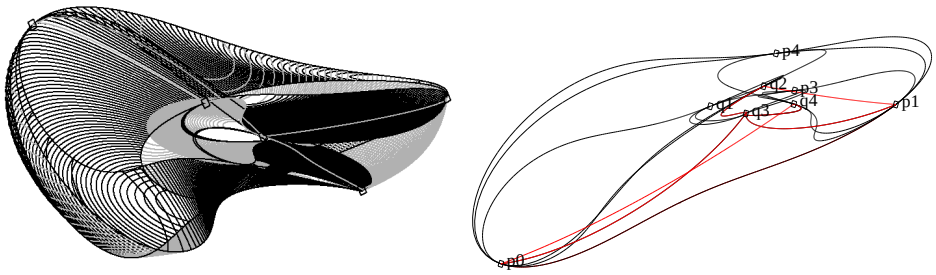

FIGURE 9. The solid torus U. On the left, we have drawn all its 2-faces, as well as its 1-skeleton. On the right, only the 1-skeleton with vertices labelled.

Note that U is G_2-invariant simply because E is so; the action of G_2 on ∂U is suggested on Figure 8 by the horizontal arrow. Our next goal is to describe a fundamental domain for the action of G_2 on U.

The Dirichlet domain has an arc in the boundary of a Giraud disk between q_1 and q_2, which is in the intersection of faces #4 and #5. By Giraud's theorem, there are precisely three bisectors containing that Giraud disk, namely the two faces #4,5 from the Dirichlet domain, as well as

$$\mathcal{C} = \mathcal{B}(G_1^{-1}p_0, G_2^{-1}G_3p_0).$$

One way to get a fundamental domain for the action of G_2 on U is to intersect U with the appropriate region between $\mathcal{C}$ and $G_2\mathcal{C}$, namely

$$D = \left\{z \in \mathbb{C}^3 : |\langle z, G_1^{-1}p_0\rangle| \leqslant |\langle z, G_2^{-1}G_3p_0\rangle|, \quad |\langle z, G_3p_0\rangle| \leqslant |\langle z, G_2G_1^{-1}p_0\rangle|\right\}$$

This turns out to give a slightly complicated fundamental domain (in particular it is not connected). We will only use $\mathcal{C}$ as a guide in order to get a simpler fundamental domain.

Proposition 6.1. *U is an embedded solid torus in $\partial_\infty \mathbf{H}^2_{\mathbb{C}}$.*

Proof: By construction, $\mathcal{C}$ contains q_1 and q_2. One easily checks by direct computation that it also contains p_2, which is given in homogeneous coordinates by $(0, 0, 1)$. One computes

$$\langle p_2, G_1^{-1}p_0\rangle = \langle p_2, G_2^{-1}G_3p_0\rangle = \frac{9 - i\sqrt{7}}{2}$$

One can study the intersection of $\mathcal{C}$ with each face of U by using the techniques of section 2.3, as in sections 4.3. The only difference is that the relevant bisectors are not all coequidistant but their intersections turn out to be disks. The result is illustrated in Figure 10 (we show the pictures that are relevant to prove these combinatorics in Figure 11).

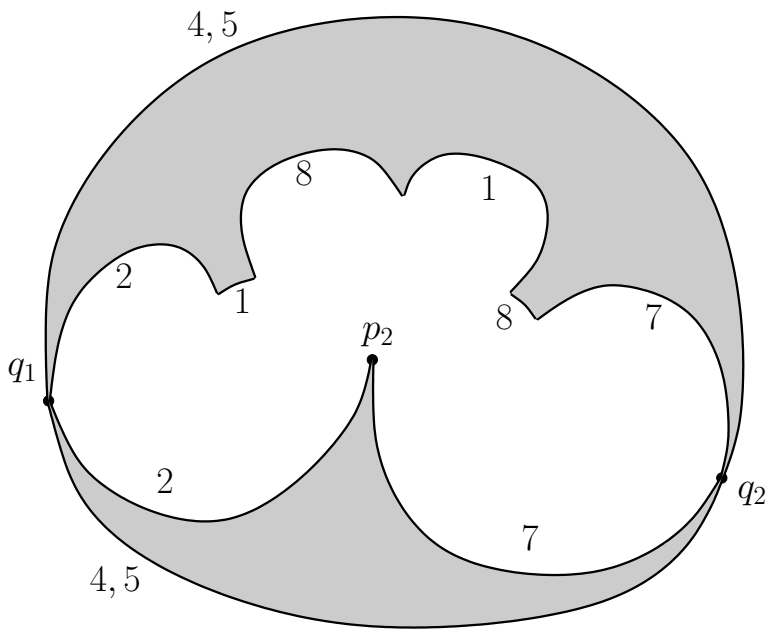

FIGURE 10. Combinatorics of the intersection of the spinal sphere $\partial_\infty \mathcal{C}$ with the Dirichlet domain. The interior of this intersection has two components, one is a topological triangle with vertices v_0, v_1 and v_4.

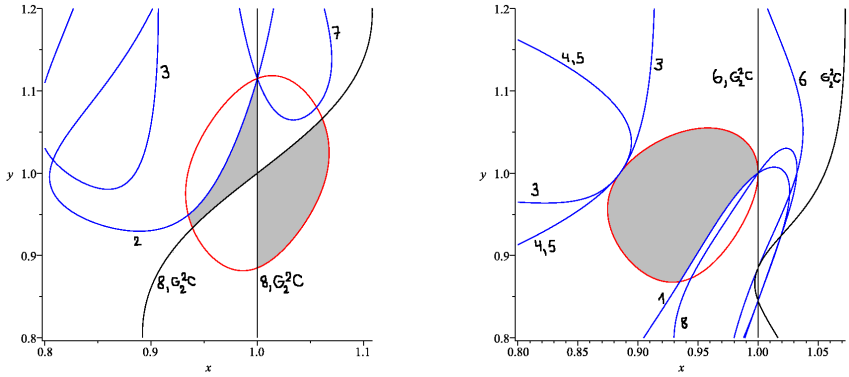

(a) $\mathcal{C} \cap \#1$ (b) $\mathcal{C} \cap \#2$

FIGURE 11. Combinatorics the intersection of $\mathcal{C}$ with some faces of the Dirichlet domain (the other ones are isometric to one of these two).

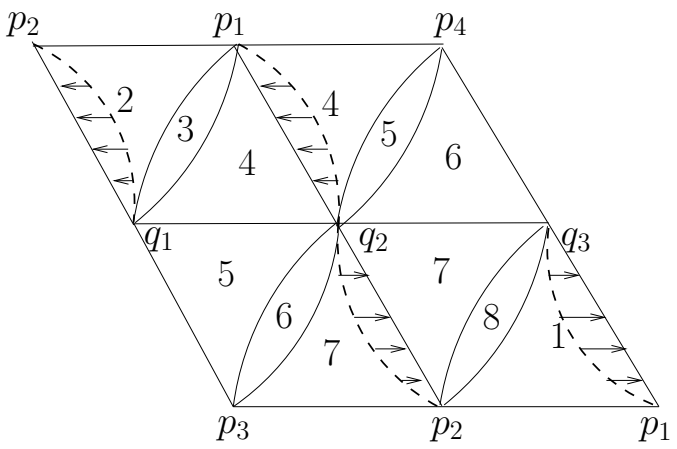

FIGURE 12. Homotopy of part of the boundary of T and $G_2(T)$ towards an arc of $\mathbb{C}$-circle.

Figure 10 clearly shows how to pick the triangle T, and it is easy to verify that T and $G_2^2(T)$ are disjoint. Moreover, they split U into two balls (they are indeed balls because they are bounded by topological embedded 2-spheres), glued along two disjoint disks. From this it follows that U is a solid torus. □

The key to getting a simple fundamental domain will be the following result.

Proposition 6.2. *The side of T from q_1 to p_2 (resp. from q_2 to p_2) is homotopic in the boundary to the arc of $\mathbb{C}$-circle joining these two points on face #2 (resp. #7). Moreover, this homotopy can be performed so that the corresponding sides of the triangle $G_2(T)$ intersect the boundary of T precisely in q_2.*

Proof: Recall the combinatorics of face #2, which is a basket as in Figure 2 with pinch points at p_1 and q_4, and whose two other vertices are p_2 and q_1. Since the side of T from q_1 to p_2 is contained in face #2 and contains no other vertex, it remains in the interior of the quadrilateral component of face #2. In that disk component, any two paths from q_1 to p_2 are homotopic, hence all of them are homotopic to the path that follows the (appropriate) arc of the $\mathbb{C}$-circle between these two points.

The argument for the other side of T is similar. The fact that the homotopies for T and $G_2(T)$ are compatible (in the sense that one can keep their sides disjoint throughout the homotopy) is obvious from the description of the combinatorics of ∂U, see Figure 12. □

The upshot of the above discussion is that we have a convenient choice of a meridian for the solid torus U, given by the concatenation of the following three arcs

- The arc of $\mathbb{C}$-circle from p_2 to q_1 which is the boundary of a slice of face #2 (only one such arc is contained in the Dirichlet domain);
- The arc of the boundary of the Giraud disk given by the intersection of the two faces #4 and #5 from q_1 to q_2 (there are two arcs on the boundary of this Giraud disk, we choose the one that does not contain p_4);
- The arc of $\mathbb{C}$-circle from q_2 to p_2 which is the boundary of a slice of face #7 (only one such arc is contained in the Dirichlet domain).

We denote this curve by σ.

Proposition 6.3. *The curve σ bounds a topological triangle $\tilde{T}$ whose interior is contained in the interior of U. This triangle can be chosen so that $\tilde{T} \cap G_2\tilde{T}$ consists of a single point, namely q_2.*

Proof: This follows from the properties of T and the homotopy from Proposition 6.2. □

7. The manifold at infinity

The results from section 6 give a simple fundamental domain for the action of Γ in the domain of discontinuity, taking the portion of U that is between T and $G_2(T)$ (and removing vertices, which are part of the limit set of Γ). We denote that region by D.

By construction, $D \cup G_2D \cup G_2^2D \cup G_2^{-1}D$ is precisely equal to the solid torus $U = \partial_\infty E$. Since we have proved that E tiles $\mathbf{H}^2_{\mathbb{C}}$, U tiles $\partial_\infty \mathbf{H}^2_{\mathbb{C}}$ (in the sense that U and γU either coincide or have empty interior). A Heisenberg view of the 1-skeleton of D is illustrated in Figure 13, and a more combinatorial one, which we will use later, is given in Figure 7.

Note that the pictures we get are not quite the same as in Figure 1 (which is the one that usually appears in the literature on the figure eight knot), but they are obtained from it by taking the mirror image.

Of course both oriented manifolds given by the usual or the opposite orientation of the figure eight knot complement admit a complete spherical CR structure. Indeed we could easily obtain the mirror image by geometric means, by replacing the representation ρ_2 by its complex conjugate representation (this would of course reverse the orientation of the quotient manifold).

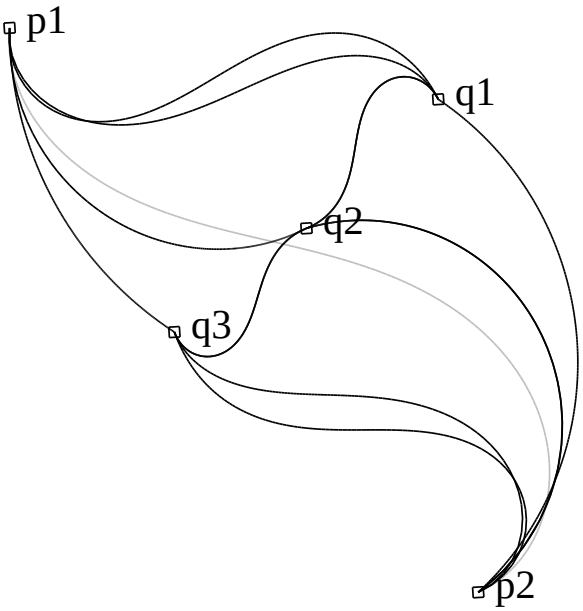

FIGURE 13. A Heisenberg view of the 1-skeleton of the fundamental domain D.

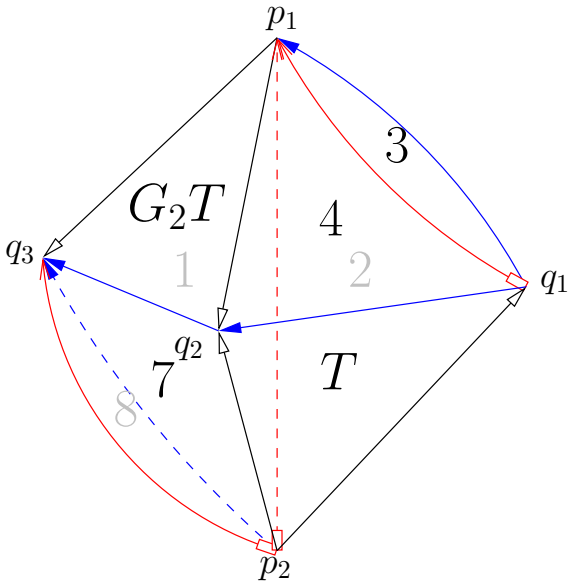

FIGURE 14. The quotient manifold is homeomorphic to a ball with identifications on the boundary, described by colored arrows.

Setting $V = \{p_1, \dots, p_4, q_1, \dots, q_4\}$, we also have that $U^0 = U \setminus V$ tiles the set of discontinuity Ω. We analyze the quotient of Ω using the side pairings, which are given either by the action of G_2 or by the side-pairings coming from the Dirichlet domain.

There are four side pairings, given in Table 4, three coming from the Dirichlet domain, and one given by G_2.

Proposition 7.1. *The maps G_1, G_2, G_3 and G_3G_1 give side-pairings of the faces of D, and map the vertices according to Table 4.*

$\#4$	$\xrightarrow{G_1}$	$\#1$
p_1, q_2, q_1		p_1, q_3, p_2
$\#2$	$\xrightarrow{G_3}$	$\#7$
p_1, p_2, q_1		q_3, p_2, q_2
$\#3$	$\xrightarrow{G_3G_1}$	$\#8$
p_1, q_1		q_3, p_2
T	$\xrightarrow{G_2}$	G_2T
p_2, q_1, q_2		p_1, q_2, q_3

TABLE 4. The four side-pairings, with their action on vertices.

Proof: The claim about G_2 holds by construction (see also Proposition 4.3). The ones about the other side-pairings come from the Dirichlet domain (where an element γ maps γ^{-1} to $\tilde{\gamma}$), provided we can prove the claims about the image of the vertices. We justify the more difficult cases by using word notation as in section 4.2. Recall the unipotent element fixing each vertex is given in Table 2; for each orbit claim, we check an explicit conjugation relation between the corresponding two unipotent elements.

$G_1(p_1) = p_1$ and $G_1(q_2) = q_3$ are obvious. The fact that $G_1(q_1) = p_2$ follows from the fact that $g_2 = [g_3, g_1^{-1}]$, since

$$1 \cdot \overline{3}2 \cdot \overline{1} = 1\overline{3}3\overline{1}\,\overline{3}1\overline{1} = \overline{3}.$$

$G_3(p_1) = q_3$ follows the fact that we just proved, which gives $G_1^{-1}(p_2) = q_1$, and conjugating by the involution I. Indeed, the conjugation relations from 4.1 imply that $I(p_2) = p_1$ and $I(q_1) = q_3$.

$G_3(p_2) = p_2$ and $G_3(q_1) = q_2$ are obvious.

The claims about G_3G_1 follow from the previous ones, since

$$G_3G_1(p_1) = G_3(p_1) = q_3$$

and

$$G_3G_1(q_1) = G_3(p_2) = p_2.$$

□

We give a simple cut and paste procedure that allows to identify the quotient as the figure eight knot complement, and this will conclude the proof of Theorem 1.1.

The procedure is illustrated in Figure 15. We slice off a ball bounded by faces #7,#8 as well as a triangle contained in the interior of D, and move it in order to glue it to face #2 according to the side pairing given by G_3^{-1}. Now we group faces #1 and #8 on the one hand, and faces #4 and #3 on the other hand, and observe that their side pairings agree to give the identifications on the last domain in Figure 15. This is the same as Figure 1 (with the orientation reversed).

8. Relationship between ρ_2 and ρ_3

In this section, we analyze the relationship between ρ_2 and ρ_3. We start by mentioning that the images of these two representations are actually conjugate subgroups of $\mathbf{PU}(2,1)$.

One can easily check that $A_1A_3^{-1}$ is regular elliptic element of order 4, hence it is tempting to take its isolated fixed point as the center of a Dirichlet domain for Γ_3 (just like we did for Γ_2, using the fixed point of G_2).

In fact it is easy to see that the corresponging Dirichlet domain is isometric to that of Γ_2, and to deduce a presentation for Γ_3, say in terms of the generators $M = A_1A_3^{-1}$ and $N = A_1$:

$$\langle M, N | M^4, (MN)^3, (MNM)^3 \rangle$$

With a little effort, these observations also produce an explicit conjugacy relation between both groups. We write

$$G_1 = \rho_2(g_1),\ G_2 = \rho_2(g_2),\ G_3 = \rho_2(g_3)$$

and

$$A_1 = \rho_3(g_1),\ A_2 = \rho_3(g_2),\ A_3 = \rho_3(g_3).$$

Denote by P the following matrix:

$$P = \begin{bmatrix} 1 & 0 & 0 \\ \frac{-3-i\sqrt{7}}{4} & \frac{-5+i\sqrt{7}}{4} & 0 \\ \frac{-1+i\sqrt{7}}{2} & \frac{-1+i\sqrt{7}}{2} & 2 \end{bmatrix}$$

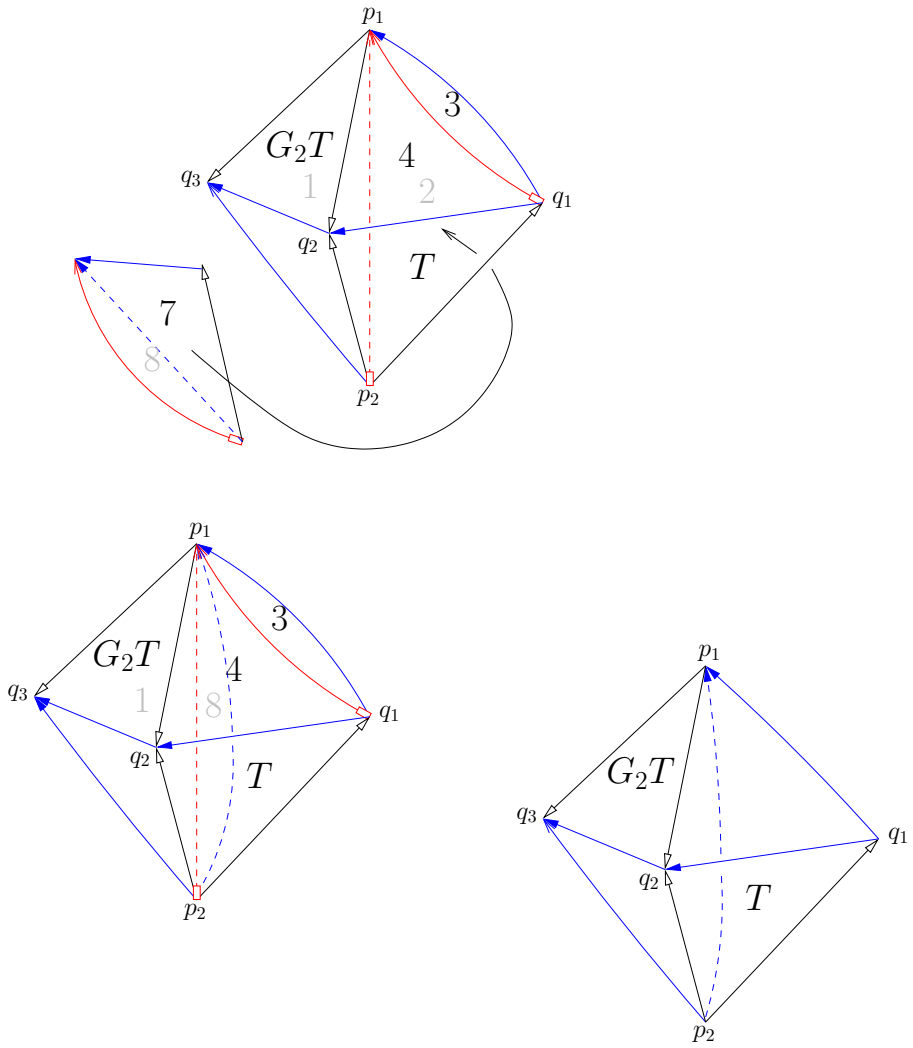

FIGURE 15. Cut and paste instructions for recovering the usual two-tetrahedra decomposition of the figure eight knot complement.

Then one easily checks (most comfortably with symbolic computation software!) that

$$P^{-1}A_1P = G_1^{-1}G_3G_1$$
$$P^{-1}A_3P = G_3$$

Note that the above two matrices generate Γ_2.

We will explain the precise relationship between the two representations ρ_2 and ρ_3 in section 9.

9. Generators for $\mathrm{Out}(\pi_1(M))$

The group $\mathrm{Out}(\pi_1(M))$ of outer automorphisms of $\pi_1(M)$ is well known to be isomorphic to the isometry group of M with its hyperbolic metric, which can be checked to be a dihedral group D_4 of order 8.

This group can in fact be visualized purely topologically in a suitable projection of the figure eight knot, for instance the one given in Figure 16.

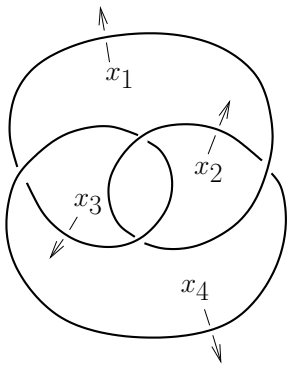

Figure 16. A symmetric diagram for the figure eight knot - there are three planes of symmetry, one being the plane containing the projection.

The Wirtinger presentation (see [12] for instance) is given by

$$\langle x_1, \dots, x_4 \mid x_4x_1 = x_3x_4,\ x_2x_3 = x_3x_1,\ x_3x_2 = x_2x_4,\ x_2x_1 = x_1x_4 \rangle.$$

We eliminate x_2, then x_3 using

$$x_2 = x_1x_4x_1^{-1}, \quad x_3 = x_2x_4x_2^{-1} \tag{4}$$

and get

$$\langle x_1, x_4 \mid x_4[x_1^{-1}, x_4] = [x_1^{-1}, x_4]x_1 \rangle.$$

It will be useful to observe that with this presentation, we can express

$$x_3 = x_1x_4[x_1^{-1}, x_4]x_1^{-1} = x_1[x_1^{-1}, x_4] = x_4x_1x_4^{-1}.$$

Of course the above presentation is the same as the one given in section 3 if we set

$$x_1 = g_3^{-1}, \quad x_4 = g_1^{-1}.$$

Using the Wirtinger presentation and an isotopy between the figure eight knot and its mirror image, for instance as suggested in Figure 17, one can check that the following elements generate $\mathrm{Out}(\pi_1(M))$.

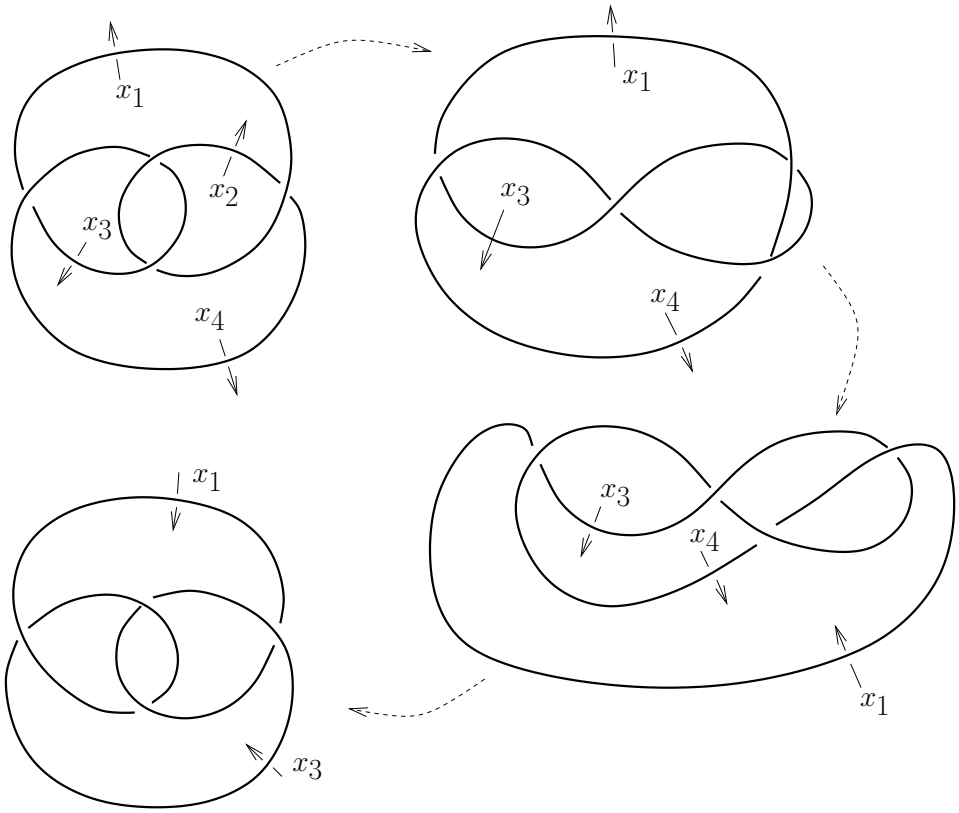

FIGURE 17. A isotopy from the figure eight knot to its mirror image.

$$\sigma : \begin{cases} g_1 \mapsto g_3 \\ g_3 \mapsto g_1 \end{cases}$$
$$\iota : \begin{cases} g_1 \mapsto g_1^{-1} \\ g_3 \mapsto g_3^{-1} \end{cases}$$
$$\tau : \begin{cases} g_1 \mapsto g_1^{-1} g_3 g_1 \\ g_3 \mapsto g_3 \end{cases}$$

Note that σ and ι correspond to orientation-preserving diffeomorphisms (and they generate a group of order 4), whereas τ reverses the orientation.

In what follows, for two representations ρ and ρ', we write $\rho \sim \rho'$ when the two representations are conjugate. We start with a very basic observation, valid for any unitary representation (not necessarily with Lorentz signature).

Proposition 9.1. *Let $\rho : \pi_1(M) \to U(2,1)$. Then $\rho \circ \iota \sim \overline{\varphi}^T$.*

Proof: For any element A of $U(2,1)$,

$$\overline{A}^T J A = J,$$

hence $A^{-1} = J^{-1}\,\overline{A}^T J$ is conjugate to $\overline{A}^T$. □

The precise relationship between ρ_2 and ρ_3 is as follows (we only give the action of $\mathrm{Out}(\pi_1(M))$ on ρ_2, since the action on ρ_3 can easily be deduced from it).

Proposition 9.2. *Let $\varphi \in Out(\pi_1(M))$. Then*

- *$\rho_2 \circ \varphi \sim \rho_2$ if and only if φ is trivial or $\varphi = \sigma\iota$.*
- *$\rho_2 \circ \varphi \sim \overline{\rho}_2$ if and only if $\varphi = \sigma$ or ι.*
- *$\rho_2 \circ \varphi \sim \rho_3$ if and only if $\varphi = \tau$ or $\iota\tau$.*
- *$\rho_2 \circ \varphi \sim \overline{\rho}_3$ if and only if $\varphi = \sigma\iota\tau$ or $\sigma\tau$.*

Proof: The fact that $\rho_2 \circ \sigma\iota \sim \rho_2$ follows from the fact that $IG_1I = G_3^{-1}$, $IG_3I = G_1^{-1}$ (see section 4.1).

One easily checks that

$$G_1^T = G_3^{-1}, \quad G_3^T = G_1^{-1}. \tag{5}$$

Now the pair G_1^{-1}, G_3^{-1} is conjugate to $\overline{G}_1^T, \overline{G}_3^T$ (because the matrices preserve J), which is conjugate to $\overline{G}_3^{-1}, \overline{G}_1^{-1}$ (by (5)), which is conjugate to $\overline{G}_1, \overline{G}_3$ (by conjugation by I). This shows that $\rho_2 \circ \iota \sim \overline{\rho}_2$.

All that is left to prove is that $\rho_2 \circ \tau \sim \rho_3$, and this was proved in section 8. □

For completeness, we give the analogous statement about ρ_1:

Proposition 9.3. *Let φ be any element of $Out(\pi_1(M))$. Then $\rho_1 \circ \varphi$ if and only if φ is in the group of order 4 generated by σ and $\iota\tau$. For all other φ, $\rho_1 \circ \varphi \sim \overline{\rho}_1$.*

Proof: In order to lighten up the notation, we write $D_1 = \rho_1(g_1)$ and $D_3 = \rho_1(g_3)$.

One easily checks that

$$ID_1I = D_3, \quad ID_3I = D_1$$

for the same involution I as in section 4.1. This shows $\rho_1 \circ \sigma \sim \rho_1$.

The key observation is that D_1 and D_3 are transpose of each other (see section 3), which together with the proof of Proposition 9.1, shows that $\rho_1 \circ \iota \sim \overline{\rho}_1$.

In order to show $\rho_1 \circ \tau \sim \overline{\rho}_1$, we simply give an explicit conjugacy. One easily verifies that

$$Q = \begin{bmatrix} 1 & 0 & 0 \\ \frac{-1-i\sqrt{3}}{2} & 1 & 0 \\ \frac{-1-i\sqrt{3}}{2} & \frac{1-i\sqrt{3}}{2} & 1 \end{bmatrix}$$

does the following:

$$Q^{-1}(G_1^{-1}G_3G_1)Q = \overline{G}_1$$
$$Q^{-1}(G_3)Q = \overline{G}_3$$

From the previous conjugacies, we have $\rho_1 \circ \iota\tau \sim \overline{\rho}_1 \circ \tau \sim \rho_1$. □

References

[1] A. F. Beardon. *The Geometry of Discrete Groups*, volume 91 of *Graduate Texts in Mathematics*. Springer-Verlag, New York, 1995.

[2] D. Burns, Jr. and S. Shnider. Spherical hypersurfaces in complex manifolds. *Invent. Math.*, 33(3):223–246, 1976.

[3] M. Deraux. Deforming the $\mathbb{R}$-Fuchsian (4,4,4)-triangle group into a lattice. *Topology*, 45:989–1020, 2006.

[4] E. Falbel. A spherical CR structure on the complement of the figure eight knot with discrete holonomy. *J. Differential Geom.*, 79(1):69–110, 2008.

[5] E. Falbel and J. Wang. Branched spherical CR structures on the complement of the figure eight knot. Preprint, 2013.

[6] W. M. Goldman. Conformally flat manifolds with nilpotent holonomy and the uniformization problem for 3-manifolds. *Trans. Amer. Math. Soc.*, 278(2):573–583, 1983.

[7] W. M. Goldman. *Complex Hyperbolic Geometry*. Oxford Mathematical Monographs. Oxford University Press, 1999.

[8] B. Maskit. *Kleinian groups*, volume 287 of *Grundlehren der Mathematischen Wissenschaften*. Springer-Verlag, Berlin, 1988.

[9] G. D. Mostow. On a remarkable class of polyhedra in complex hyperbolic space. *Pacific J. Math.*, 86:171–276, 1980.

[10] J. R. Parker and P. Will. A family of spherical CR structures on the Whitehead link complement. in preparation.

[11] M. Phillips. Dirichlet polyhedra for cyclic groups in complex hyperbolic space. *Proc. Amer. Math. Soc.*, 115:221–228, 1992.

[12] D. Rolfsen. *Knots and links*, volume 7 of *Mathematics Lecture Series*. Publish or Perish Inc., Houston, TX, 1990.

[13] R. E. Schwartz. Degenerating the complex hyperbolic ideal triangle groups. *Acta Math.*, 186(1):105–154, 2001.

[14] R. E. Schwartz. Real hyperbolic on the outside, complex hyperbolic on the inside. *Inv. Math.*, 151(2):221–295, 2003.

[15] R. E. Schwartz. *Spherical CR geometry and Dehn surgery*, volume 165 of *Annals of Mathematics Studies*. Princeton University Press, 2007.

[16] W. P. Thurston. The Geometry and Topology of Three-Manifolds. http://library.msri.org/books/gt3m, 2002. Princeton lecture notes.

Martin Deraux
Institut Fourier, Université de Grenoble 1, BP 74, Saint Martin d'Hères Cedex, France
deraux@ujf-grenoble.fr
Elisha Falbel
Institut de Mathématiques, Université Pierre et Marie Curie, 4 place Jussieu, F-75252 Paris, France
falbel@math.jussieu.fr